Gas Target Design and Characterisation for EPAC EA1

Contact: oliver.finlay@stfc.ac.uk

O.J. Finlay, N. Bourgeois, A. Stallwood, D.R Symes
Central Laser Facility, Rutherford Appleton Laboratory, Didcot, OX11 0QX, UK

X.J. Gu, B. John, D.R Emerson
Scientific Computing Department, STFC Daresbury Laboratory, Warrington, WA4 4AD, UK

L. Feder
John Adams Institute for Accelerator Science and Department of Physics, University of Oxford, Denys Wilkinson Building, Keble Road, Oxford OX1 3RH, UK

1 Introduction

Experimental Area 1 (EA1) in the Extreme Photonics Applications Centre (EPAC) will predominantly support experiments which utilise a long focal length parabola to focus the laser onto a gas target to generate high energy electrons and x-rays. The gas density profile can be tailored to favour the accelerator properties required for a particular application. The EPAC facility will provide users with a number of facility designed, characterised and maintained options for gas targetry depending on their requirements. The first objective for the EPAC gas target design programme has been to manufacture and characterise a supersonic rectangular slot nozzle, with a length scalable up to 200 mm. This choice was based on the LBNL result using 200 mm acceleration length to achieve 8 GeV electron energies [1] and the demonstration of HOFI guiding channels in a 200 mm long gas jet target by the Maryland group using the ALEPH laser at CSU [2]. A jet has been chosen over a gas cell for a first design due to their inherent robustness and simplicity. Fluid modelling that has been performed for a 40 mm long gas nozzle is detailed in section 2. The simulated design has been manufactured and preliminary characterisation work to verify the simulation results will be presented in section 3.

2 Gas Jet Design

The first step in the EPAC gas jet design programme was to design a gas nozzle compatible with experiments in Gemini TA3, with a length of 40 mm and backed by a single valve inlet. Slot-shaped gas nozzles have been used by several groups in the laser-plasma community [3, 4] and drawing from their experience, an initial outline was conceived. The outline consisted of a solenoid valve backing a reservoir, from which gas flows evenly through a converging-diverging section in the narrow direction of the slot. This section accelerates the gas to supersonic velocities, which is necessary to condition the flow and minimise the transverse spreading of the gas as it exits the nozzle.

Typically, the orifice diameter of a high pressure solenoid valve is, at most, a couple of millimetres and our design relies on an evenly-filled reservoir with a cross-sectional area on the order of the nozzle exit area to generate a flat density profile above the nozzle. Fluid simulations were performed in Code-Saturne [5], which is an open source code capable of 3D fluid modelling, to model this situation. Figure 1 shows a simulation of the gas (helium) density distribution when a small inlet, with diameter 1.2 mm (imitating a Peter-Paul Solenoid valve [6]) and a backing pressure of 20 bar, is attached to a larger chamber. In the lower chamber, a large spike in the density is seen directly above the inlet due to a locally lower gas temperature. In order to mitigate this, a baffle plate is added above the lower chamber. This blocks the gas directly from the inlet and allows it to flow into an upper chamber through holes not lined up with the central axis. In the upper chamber (separate colourbar) it can be seen that the density profile is more uniform. Although further optimisation of the baffle plate can be be done to further homogenise the density profile in the upper chamber, this simulations provides a proof of concept demonstration of the technique.

With this solution implemented, simulation of the supersonic nozzle could be performed. The basic principle involves an initial converging section, over which the gas is accelerated to the speed of sound at the region of minimum width: the throat. As the gas travels from the throat through the diverging section, it accelerates to supersonic velocities. For simplicity in design and in manufacture, it was decided that the taper angle in both of these sections would be equal and would be constant through the nozzle. The scaling laws dictate that for a nozzle like this, for a small taper angle, the Mach number is proportional to the area difference between the nozzle throat and the nozzle exit [7, 8]. The higher the Mach number, the smaller the density drop between the nozzle exit and the region a few millimetres above, where the drive laser will likely interact with the gas. Another consideration is the efficiency of transfer of gas density at the nozzle throat to the nozzle exit. This efficiency

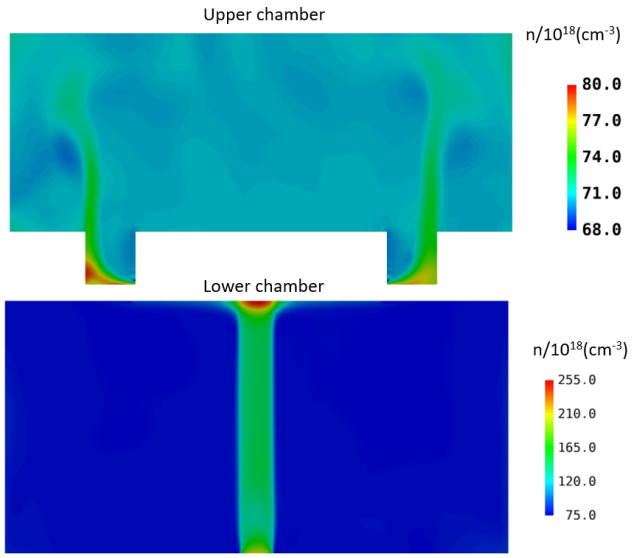

Figure 1: Simulation showing the gas density when gas flows from a small inlet into a large chamber. The density profile is made more uniform in the upper chamber using a baffle plate to block the flow directly above the inlet.

is inversely proportional to the area difference between the nozzle throat and the nozzle exit because for a given throat width and backing pressure, a fixed amount of gas passes through which spreads out over the nozzle exit area. These considerations need to be balanced to maximise the efficiency of achieving a certain density at a given height above the gas. The final design has a throat width of 300 μm and an exit width of 2 mm to give a Mach number at the nozzle exit of 3.5. CAD drawings, showing the designed nozzle and showing the cross-section are shown in figure 2. The lower section of the nozzle has been designed to fit to a Peter-Paul solenoid valve.

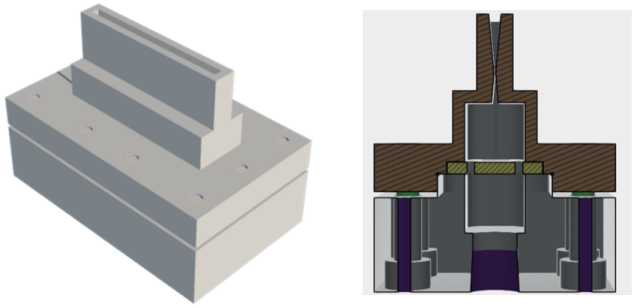

Figure 2: CAD drawing of designed slot nozzle.

3D fluid simulations were performed with this design. The inlet diameter was 1.2 mm, from which the gas flowed into a lower chamber, through the baffle plate and then through the converging-diverging section of the nozzle with length 40 mm. The gas was helium and 10 bar, 20 bar, and 30 bar backing pressures were simulated at the inlet. The longitudinal gas density profile at a height of 5 mm above the nozzle is shown in figure 3 at these pressures at different times. A quasi steady state is achieved by 10 ms after the valve opening time but, particularly for higher backing pressures, the profile varies with time. Also for higher pressures, the profile is not entirely flat. This is most likely due to non-uniformities in the gas density profile below the converging-diverging section. Through careful optimisation of the baffle plate design, it is hoped that the uniformity can be improved. The scaling of the density with height is plotted in figure 4.

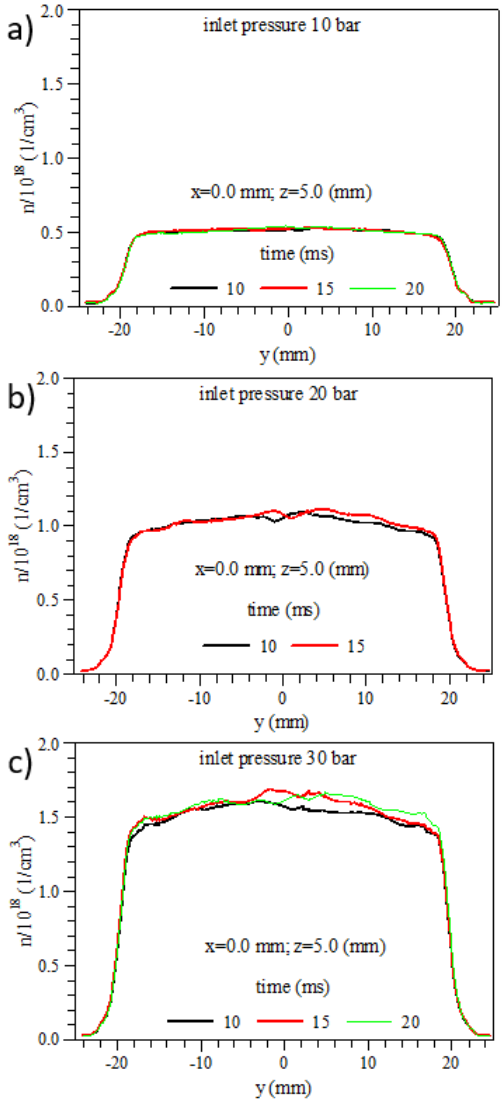

Figure 3: Simulated longitudinal gas density profile with a) 10 bar, b) 20 bar and c) 30 bar backing pressures at different times.

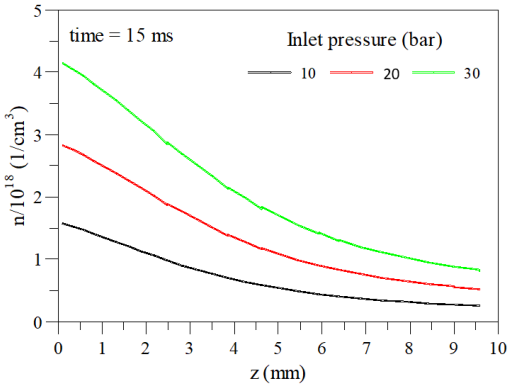

Figure 4: Simulated gas density with height for 10 bar, 20 bar and 30 bar backing pressures at 15 ms after valve opening.

Manufacturing tolerances were not considered in the simulation. The dimension most likely to see large percentage deviations from the design specification is the nozzle throat, which is 300 μm over the nozzle length. Few percentage deviations over the length will affect the uniformity of the density profile. The technique chosen for the manufacturing of this nozzle design was Electric Discharge Machining with a wire. The quoted manufacturing tolerance on the throat width deviation was $\pm 3\,\mu$m. Once the nozzle was made, the throat width was measured to confirm it met the specification. The result is shown in figure 5. The mean width is 305.6 μm with a standard deviation along the 40 mm length of 2.9 μm. The measurement error was on the order 3 μm. The plot shows that only one measurement point, at 21 mm, is not inside the $\pm 3\,\mu$m manufacturing tolerance range given measurement errors. Further work is required to investigate whether the drop in the measured width at 21 mm affects the gas density profile.

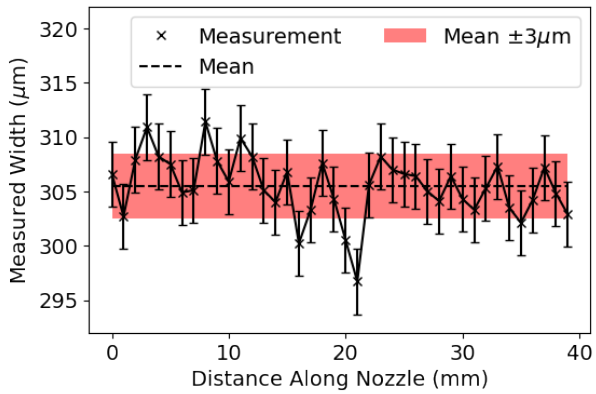

Figure 5: Measurement of the nozzle throat width. The mean width is 305.6 μm with standard deviation of 2.9 μm.

3 Gas Jet Characterisation

A neutral gas interferometry rig has been established in Gemini Target Area 1 (TA1) for characterisation of the gas targets. The initial design imitated Ref. [9], where a blue laser passed through the gas plume 4 times to accumulate more phase shift and achieve high density sensitivity. Argon is used as it has a larger refractive index than helium but has the same heat capacity ratio, hence similar flow properties. A diagram of the setup in TA1 is shown in figure 6. A linearly polarised blue diode laser is expanded to a diameter of 30 mm where it passes through a 50/50 beamsplitter and is transmitted through a polarising beamsplitter before it passes through the gas plume. The beam is retro reflected, with a pair of lenses in the line to image the jet and phase information back onto itself. In this line, two passes through a quarter waveplate flips the laser polarisation such that, after the second pass through the gas plume, the polarising beamsplitter reflects the beam to a second image relay. The beam then propagates past the jet a third time and is retro reflected through the first image relay line to achieve the fourth pass. The quarter waveplate flips the polarisation again so it transmits though the polarising beamsplitter and is extracted via the 50/50 beamsplitter before being imaged onto the camera. The phase information is measured with a Nomarski interferometer, consisting of a Wollaston prism and a polariser in front of the camera.

To characterise the stability of this setup, 50 reference images were taken without gas. Each interferogram was filtered with a 2D continuous wavelet transform [10] and the phase was unwrapped using the unwrap phase function in scikit-image. The stability of the phase was characterised by first taking the standard deviation of the unwrapped phase over all of the reference images, which gave a 2D map of the phase deviation. This map has hot spots due to defects in the beam profile or in the phase retrieval process. In order to quantify and compare phase stability in different scenarios, the median was taken of the 2D phase deviation. Figure 7 plots this median phase deviation for three different cases: the four pass interferometer setup, as drawn in figure 6, for the four pass interferometer with a makeshift foil covering over the interferometer and with a two pass interferometer (removing the quarter waveplate). The standard four pass interferometer has a median phase deviation of 100 mrad. This can be reduced by twenty percent by covering the region between the Wollaston prism and the camera, i.e. where the pulse is split, with matte black foil in an attempt to reduce air currents in the region. The median phase deviation of the two pass system is 34 mrad. The two pass system has less than half the path length of the four pass system and fewer optics, which appears to be advantageous for phase stability. Taking this median phase deviation as a metric of minimum phase sensitivity, these three scenarios have a density sensitivity per

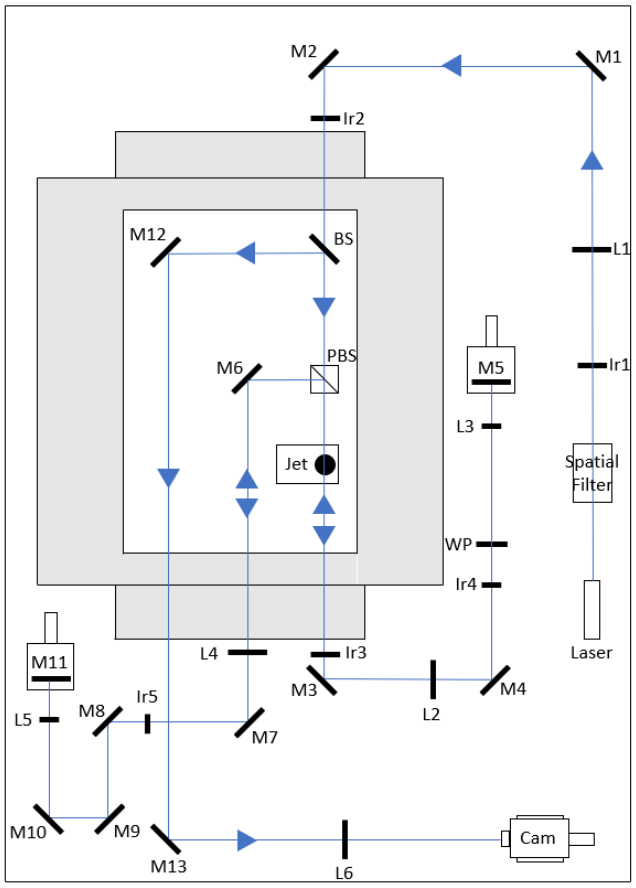

Figure 6: Diagram of four pass interferometry setup. The shaded area denotes the vacuum chamber. M = Mirror, L = Lens, Ir = Iris, BS = Beamsplitter, PBS = Polarising Beamsplitter, WP = Quarter Waveplate.

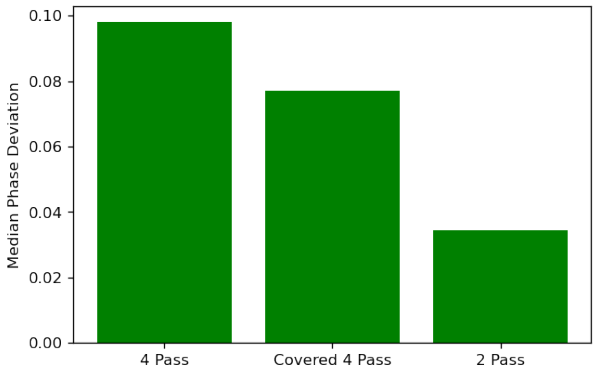

Figure 7: Median phase deviation, as defined in the text, for the four pass interferometer, the four pass interferometer with a foil covering over the region between the Wollaston prism and the camera, and for a two pass interferometer (removing the quarter waveplate).

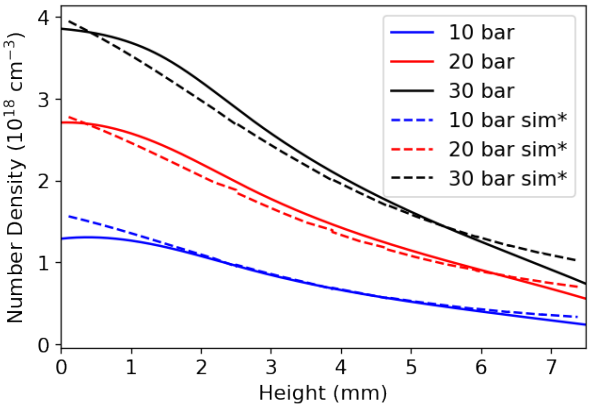

Figure 8: Neutral gas density measurement with probe traversing long direction of 40 mm EPAC slot nozzle. Simulation scaled to match inefficiency in gas line experimentally.

centimeter of length in the probe direction of travel of $1.9 \times 10^{16}\,\mathrm{cm}^{-2}$, $1.5 \times 10^{16}\,\mathrm{cm}^{-2}$ and $1.3 \times 10^{16}\,\mathrm{cm}^{-2}$ respectively.

Using the interferometer in a two-pass configuration, the density profile produced by the 40 mm EPAC design gas nozzle was measured with the probe traversing the long direction of the jet. The density profile in the probe direction was assumed to be constant over a 40 mm length. Figure 8 compares the experimental measurement to the simulation. Although the simulation models the nozzle geometry accurately, it does not account for loss in the gas line between the gauge and the solenoid valve. For this reason, the simulation results were scaled by a factor of 1/2 to match the amplitude of the experimental measurement. The scaling of density with height appears to be consistent in simulations and experiment.

Measurement of the phase profile in the perpendicular direction was not possible with this Nomarski interferometer geometry. With this geometry, the beam passes through the gas jet, which is later split, and separate parts of that beam are interfered to generate the shifted phase profile. From this alone, there is a maximum of 15 mm field of view for density measurements in this setup (i.e. half the full beam size). Another limitation is that changing the beam separation requires a movement of the Wollaston prism with respect to the camera, which also changes the fringe frequency. In this setup, the Wollaston prism positions for which the fringe frequency was low enough that an appropriate contrast was seen corresponded to a beam separation of significantly less than 15 mm, hence a smaller field of view in practice. Given the stated limitations of the current interferometric density characterisation rig, an upgrade is underway. This will be a two pass interferometer with a separate reference arm to allow density measurement over the full beam size. Since the coherence length and spatial quality of the blue diode laser used in these measurements

could be limiting in this new geometry, a helium-neon laser will be used instead.

4 Conclusion and Outlook

Design and characterisation of gas targetry to be used at the EPAC facility has begun. Fluid simulations have been performed to design a prototype rectangular gas jet nozzle, which has been manufactured. Preliminary characterisation has been done on the manufactured nozzle by measurement of the nozzle throat size, and of the density profile through interferometry. This first design provides a simple, flat density profile with one gas inlet. In order to extend the length of the nozzle, and hence increase the volume over which a certain gas density is required, multiple inlets can be added to increase gas flow, as in Ref. [3]. Future designs also aim to control injection through shock injection or truncated ionisation injection.

References

[1] A. J. Gonsalves et al. Petawatt Laser Guiding and Electron Beam Acceleration to 8 GeV in a Laser-Heated Capillary Discharge Waveguide. *Phys. Rev. Lett.* **122,** (8 2019), p. 084801.

[2] B. Miao et al. Multi-GeV Electron Bunches from an All-Optical Laser Wakefield Accelerator. *Phys. Rev. X* **12,** (3 2022), p. 031038.

[3] J. E. Shrock et al. Meter-scale plasma waveguides for multi-GeV laser wakefield acceleration. *Physics of Plasmas* **29,** 7 (July 2022), p. 073101.

[4] K v. Grafenstein et al. Laser-accelerated electron beams at 1 GeV using optically-induced shock injection. *Scientific Reports* **13,** (1 2023), p. 11680.

[5] Frédéric Archambeau, Namane Méchitoua, and Marc Sakiz. Code_Saturne: a Finite Volume Code for the Computation of Turbulent Incompressible Flows. *International Journal on Finite Volumes* **1,** (2004).

[6] *Peter Paul*. `https://peterpaul.com/valves/2-way-normally-closed/series-20-model-eh22`.

[7] S. Semushin and V. Malka. High density gas jet nozzle design for laser target production. *Review of Scientific Instruments* **72,** 7 (July 2001), pp. 2961–2965.

[8] K. Schmid and L. Veisz. Supersonic gas jets for laser-plasma experiments. *Review of Scientific Instruments* **83,** 5 (May 2012), p. 053304.

[9] Stefan Karatodorov et al. Multi-pass probing for high-sensitivity tomographic interferometry. *Scientific Reports* **11,** (1 2021), p. 15072.

[10] Paolo Tomassini et al. Analyzing laser plasma interferograms with a continuous wavelet transform ridgeextraction technique: the method. *Appl. Opt.* **40,** 35 (2001), pp. 6561–6568.